Open Journal of Geology, 2023, 13, 171-188
https://www.scirp.org/journal/ojg
ISSN Online: 2161-7589
ISSN Print: 2161-7570

Integrating Aster Images Processing and Fieldwork for Identification of Hydrothermal Alteration Zones at the Oumjrane-Boukerzia District, Moroccan Anti-Atlas

Lhoussayn Ouhoussa[1], Abdessamade Ghafiri[1], Lakhlifa Ben Aissi[2], Brahim Es-Sabbar[2]

[1]LGAGE Laboratory, Department of Geology, Faculty of Sciences Ben M'sick, University Hassan II, Casablanca, Morocco
[2]Applied Geology Laboratory, Department of Geosciences, Faculty of Sciences and Technics, Moulay Ismail University, Errachidia, Morocco
Email: l.ouhoussa@gmail.com

How to cite this paper: Ouhoussa, L., Ghafiri, A., Aissi, L.B. and Es-Sabbar, B. (2023) Integrating Aster Images Processing and Fieldwork for Identification of Hydrothermal Alteration Zones at the Oumjrane-Boukerzia District, Moroccan Anti-Atlas. *Open Journal of Geology*, **13**, 171-188.
https://doi.org/10.4236/ojg.2023.132008

Received: January 14, 2023
Accepted: February 17, 2023
Published: February 20, 2023

Abstract

Mapping from remote sensing has become more effective in the field of geology, mainly in lithological discrimination and identification of hydrothermal alteration zones. The use of this technique consists in obtaining information about the rock mass and the main ones existing in the inaccessible areas. Satellite data from the ASTER (Advanced Spaceborne Thermal Emission and Reflection Radiometer) sensor represent a favorable potential for detecting the spectral signatures of mineral zones and identifying their nature. These data are more reliable in places where the climate is arid with less abundant vegetation, as at the Oumjrane-Boukerzia mining district. This region which is part of the Eastern Anti-Atlas, is composed of several mineralized veins which still require detailed studies and exploration by the technique of remote sensing. In this work we applied several processing techniques on ASTER imagery such as Colored Composition, Principal Component Analysis and Ratio Bands. The use of the reports of the specialized Bands makes it possible to identify some hydrothermal alteration minerals within the mining district of Oumjrane Boukerzia. These minerals are represented mainly by iron oxides and hydroxides (Hematite, jarosite, limonite and goethite), carbonate minerals (dolomite, calcite), clay minerals (Illite, kaolinite and chlorite) and quartz minerals. This work allows us to produce a map of hydrothermal alteration zones which can be used as a valuable reference in the strategy of mining exploration for the base metals (Cu, Pb, Zn and Ba), in the mining district of Oumjrane-Boukerzia and in the entire Eastern Anti-Atlas.

Keywords

Anti-Atlas, Oumjrane-Boukerzia, Alteration, Mineral, ASTER, Remote Sensing

1. Introduction

The use of remote sensing data, particularly ASTER data, has become more important, especially in the mapping of hydrothermal alteration zones [1]. This data provides more effective information that can help mining exploration geologists, due to the spatial, spectral and radiometric variability and resolution of this image [2]. While the identification of areas that have undergone hydrothermal alteration in the field of mining prospecting requires other important techniques, in this case the exploitation of ASTER data can provide cost-effective solutions for the search for new exploration areas mine before detailed and costly ground investigations [3]. Many studies have been carried out on the mapping of hydrothermal alteration zones using ASTER imagery [4].

The mining district of Oumjrane-Boukerzia is located in the southwestern part of the Moroccan Anti-Atlas (**Figure 1(a)**). This region is characterized by an arid climate with absence of vegetation cover, thing that makes it favorable environment for remote sensing investigations, in particular geological mapping. In addition, the Oumjrane-Boukerzia region is well known for its significant mineral potential hosted within the sandstones of the second Bani group of upper Ordovician age. These mineral deposits are represented by a set of mineralized veins filled with copper and lead sulfides, and barite. This vein system is represented mainly by the Bounhas (Cu, Pb), Afilou n'Khou (Cu), Rich Merzoug (Cu, Ba) and Boukerzia (Pb, Cu, Ba) veins [5]. Most of the studies that have been carried out in the Oumjrane-Boukerzia mining district concern mostly the stratigraphy, and paleontological characterization of the Paleozoic outcrops [6] [7]. The [8] have established an excellent geological map of different outcrops and major faults in this part of Anti-Atlas. Then, structural analysis has been made by [9] at the Eastern Anti-Atlas scale, and at the Maider Basin scale by [5] and [10] where they highlight a remarkable NE-trending Variscan shortening of late carboniferous-lower Permian age, which is responsible for the region structuring. The [2] and [11] have performed in this region lithological and fractures mapping based on Landsat 8 OLI image processing. On the scale of the Eastern Anti-Atlas, the Paleozoic terrains are home to several mineral zones, mainly in the form of veins [5] [12]. This makes the implement of remote sensing of extreme importance for alteration mineral zones. However, no remote sensing work on the delimitation of the alteration zones and identification of the main minerals associated with the copper deposit of Oumjrane-Boukerzia has been published, except the work of that concern the lithological and fractures mapping [2].

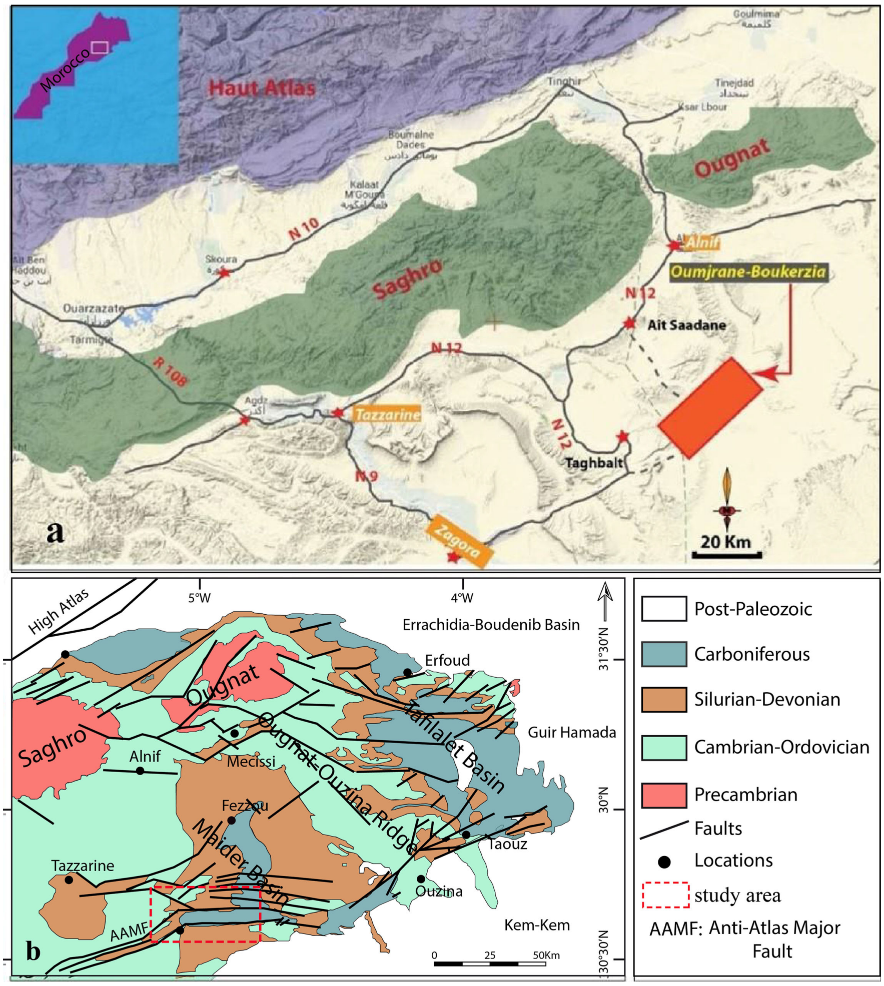

Figure 1. (a) Location of the study area; (b) location of the Oumjrane-Boukerzia mining district in the eastern Anti-Atlas map [15].

The present paper aims to process the spectral bands of ASTER imagery to map the areas of hydrothermal alteration at the Oumjrane-Boukerzia region. The obtained results will be validated by field work survey, in order which ultimately establishes a map of alteration mineral zones. In addition, and we will superimpose the results with the fracturing map to examine the spatial relationship between the main fractures and the obtained alteration mineral zones. Finally, the major objective is to guide mining exploration work towards areas potentially favorable for mineral concentrations (Cu, Pb, Zn and Ba).

2. Geological Setting

The Eastern Anti-Atlas is made up of a Precambrian basement forming thus two inliers: Saghro and Ougnat, surrounded by a Paleozoic cover. The Eastern Anti-Atlas is separated from the High Atlas by the Cretaceous Ouarzazate and Errachidia Basins. These two Precambrian inliers are surrounded by a 4 - 5 km thick Paleozoic sedimentary layers, which are formed, on the southern and eastern sides of the Saghro-Ougnat axis, by the Maider and Tafilalet basins, respectively.

The Eastern Anti-Atlas is characterized by a superposition of tectonic events resulting in major-oriented structures that are the Anti-Atlas E-W and the Ougartien NW-SE directions [9] [13]. These two tectonic events affect the Tazzarine, Maider and Tafilalet basins. The Precambrian basement underwent a shortening during the Variscan orogeny resulting in the Paleozoic cover folding (disharmony in the Adoudounian which plays the role of plastic layer and favorable surface of detachment folds). Subsequently, the folds were only rarely replied during the Alpine orogeny. As in the High Atlas, the Anti-Atlas foreland belt was uplifted in response to the N-S trending Alpine compression [14].

The Paleozoic sedimentary pile was deposited in shallow water and contains a reduced Lower Cambrian shales and conglomerates, followed by Middle Cambrian, Ordovician, and Silurian alternating shales and sandstone. This monotonous terrigenous succession is overlaid by a Devonian Carbonate platform with detrital Carboniferous succession. This thick series was subjected to an extensional event during the Middle-Upper Devonian period [15], and was later deformed by the Variscan shortening, which is mostly directed NE-SW and induced the reactivation of the former normal faults [9].

The Oumjrane-Boukerzia mining district is located in the eastern Anti-Atlas, 50 kilometers south of Alnif town and 90 kilometers northeast of Zagora city. It has a NE-SW management zone that is 40 km long and 10 km broad. This huge territory (400 km^2) is situated at the western part of the Maider basin, in the southeast of Jbel Saghro. It is part of the Maider and Tafilalet vein field, and it is made up of Lower and Upper Paleozoic units. This Paleozoic cover is sub-horizontal and heavily faulted, with large-wavelength folds bordered by the major fault affecting the area. These terrains are locally intruded by a set of basic dikes with three directions; E-W, NE-SW and NW-SE [5]. The Bounhas copper deposit is the most economically significant deposit in the whole Oumjrane-Boukerzia mining district, with big metals stocks. The mineralized structures of the Bounhas deposit are of lenticular vein-type, extending about 3 km in an E-W direction with steeply south-dipping. The mineralization associated with this deposit is hosted in sandstones and quartzites of the second Bani formation of the Upper Ordovician [10] (**Figure 1(b)**).

3. Data and Methods

3.1. Data

The data source used in this work corresponds to the ASTER images downloaded for free from the website (https://gbank.gsj.jp/madas/map/), covering the region of Oumjrane-Boukerzia acquired on April 01 2021, obtained from “Land Process Distributed”, NASA active archive center. These images have already been georeferenced to the UTM (Universal Transverse of Mercator) projection using the WGS-84 ellipsoid. The Aster Images are composed of 14 spectral bands grouped into three domains (VNIR: Visible and Near-Infrared; SWIR: Short-Wave Infrared; TIR: Thermal Infrared). In this work we used the ASTER satellite image to detect and identify the hydrothermal alteration zones of the Oumjrane Boukerzia mining district. In this paper, all processing was carried out using ENVI (Environment for Visualizing Images, http://www.exelisvis.com) software version 5.1, and ArcMap version 10.2 software. The topographic of Fezzou and the 1:200,000 geological maps of Toudgha-Maider [6] served as reference maps and guide during the first validation of the obtained results from this processing of Aster images. The technical characteristics of the "ASTER sensor" remote sensing are summarized in Table 1.

3.2. Methods

After downloading the images, the first step consists of the pre-processing of these images applying radiometric and atmospheric correction. Subsequently, a processing step, composed by several techniques, was applied to the spectral bands of the ASTER images such as the colored composition, the principal component analysis and the band ratio technique, in order to improve the visibility and the quality of images [2]. The validation of the results was carried out in two steps: the first is based on the spectral signature of the USGS (United States Geological Survey) library to separate between the minerals presented in the study area, the second step is based on direct field observations in order to determine the family of minerals abundant in the bedrock, which is served as the basic elements of the identified zones. The adopted methodology approach for this work is illustrated by Figure 2.

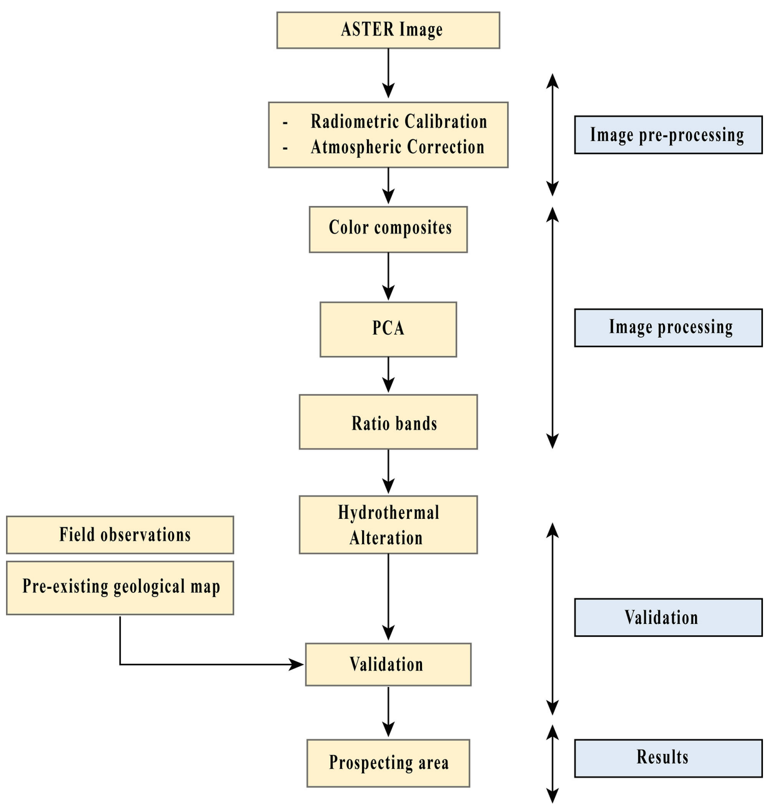

Figure 2. Flowchart showing the main steps of the methodology approach.

Table 1. The characteristics of the ASTER image [16].

ASTER Specification			
Instrument	VNIR	SWIR	TIR
Bands	Band1-Band3	Band4 - Band9	Band10 - Band14
Spectral range (μm)	0.52 - 0.60 0.63 - 0.69 0.78 - 0.86	1.600 - 1.700 2.145 - 2.185 2.185 - 2.225 2.235 - 2.285 2.295 - 2.365 2.360 - 2.43	8.125 - 8.475 8.475 - 8.825 8.925 - 9.275 10.25 - 10.95 10.95 - 11.65
Spatial resolution	15 m	30 m	90 m
width and length	60 km	60 km	60 km
Cross pointing	±318 km (±24 deg)	±116 km (±8.55 deg)	±116 km (±8.55 deg)
Signal quantization level (bits)	8	8	12

4. Image Processing

4.1. Color Composite

Examination of a single band within a period of time does not give precise information on the lithological nature of the facies presented in the area. In this case the combination between several spectral bands makes it possible to identify the spectral characteristics in detail on the different types of outcrops in the study area. It allows to represent a group simultaneously on the image processing system, which allows to produce a more useful and efficient multi-band image. The application of color composition (RGB) on the satellite image ASTER is very useful for hydrothermal alteration mapping [16]. In the present work, the colored compositions (RGB SWIR 468) **Figure 3(a)** and RGB SWIR 578 **Figure 3(b)** have been applied to the ASTER satellite image covering the Oumjrane-Boukerzia area. These two combinations depict satisfied results for geological mapping, especially the identification hydrothermal alterations (**Figure 3**).

4.2. Principal Component Analysis

Many RGB combinations were carried out on the main components resulting from the processing of ASTER images, including the purpose of discriminating between lithological facies of study area, and the identification of areas that may undergo hydrothermal alterations [17]. In this study, the PCA combination (PC5, PC4 and PC3) **Figure 4(a)** and (PC6, PC4 and PC1) **Figure 4(b)** as (RGB mode) represent the best result. It allows to differentiate between second Bani sandstones (red color) and Ktaoua shales (open green color) (**Figure 4**). These geological formations are affected by most of the mineralized faults in this area, which makes it possible to generate several alteration minerals. Indeed, these lithological units are the main host rock of the mineralization (Cu, Ba, Pb) presented in the study area. Therefore, the identification of these facies helps the exploration teams to easily detect the different mineral occurrences exposed in the area.

5. Results

5.1. Index of Iron Oxides and Hydroxides Minerals

In this case part of the electromagnetic wavelength belongs to the domains of VNIR and SWIR, was used for the detection of iron oxide and hydroxide minerals, these minerals have appeared in weathered rocks generally of reddish and blackish color, this aspect is mainly related to the presence of a mineral concentration rich in ferric iron elements (Fe^{3+}) [3]. These iron oxides and hydroxides are mainly represented by hematite, goethite, limonite and jarosite. These minerals show high reflectance in the visible red (band3) about 0.78 to 0.86 um, with

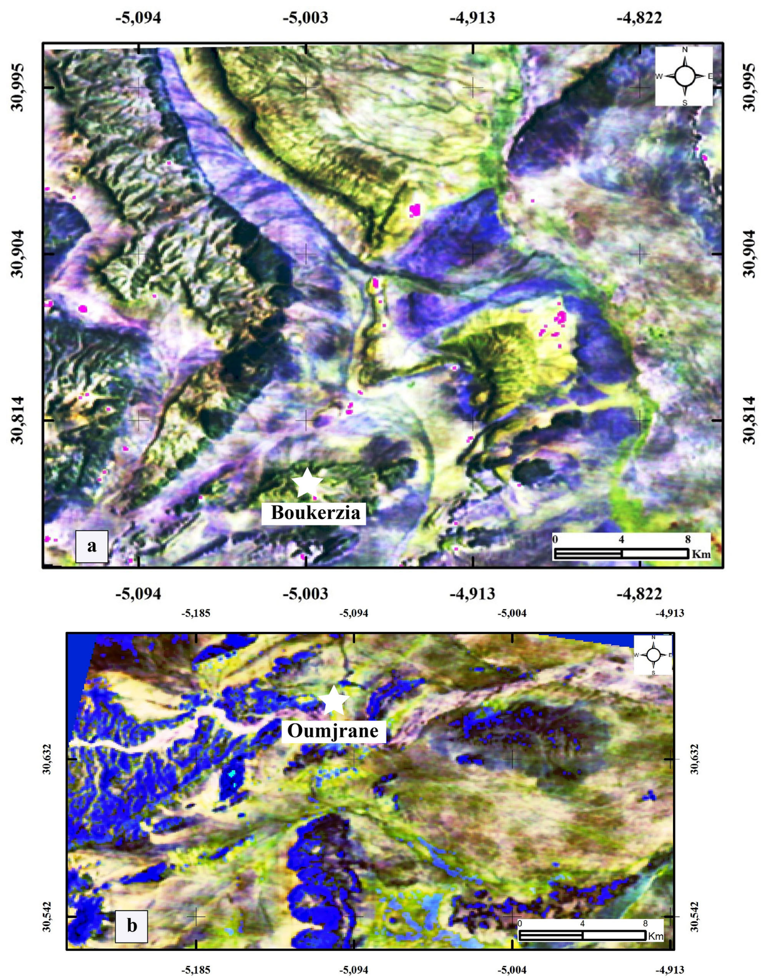

Figure 3. Colored compositions applied to the ASTER images: (a) RGB colored composition (468) at Boukerzia zone, (b) RGB colored composition (578) at Bounhas zone.

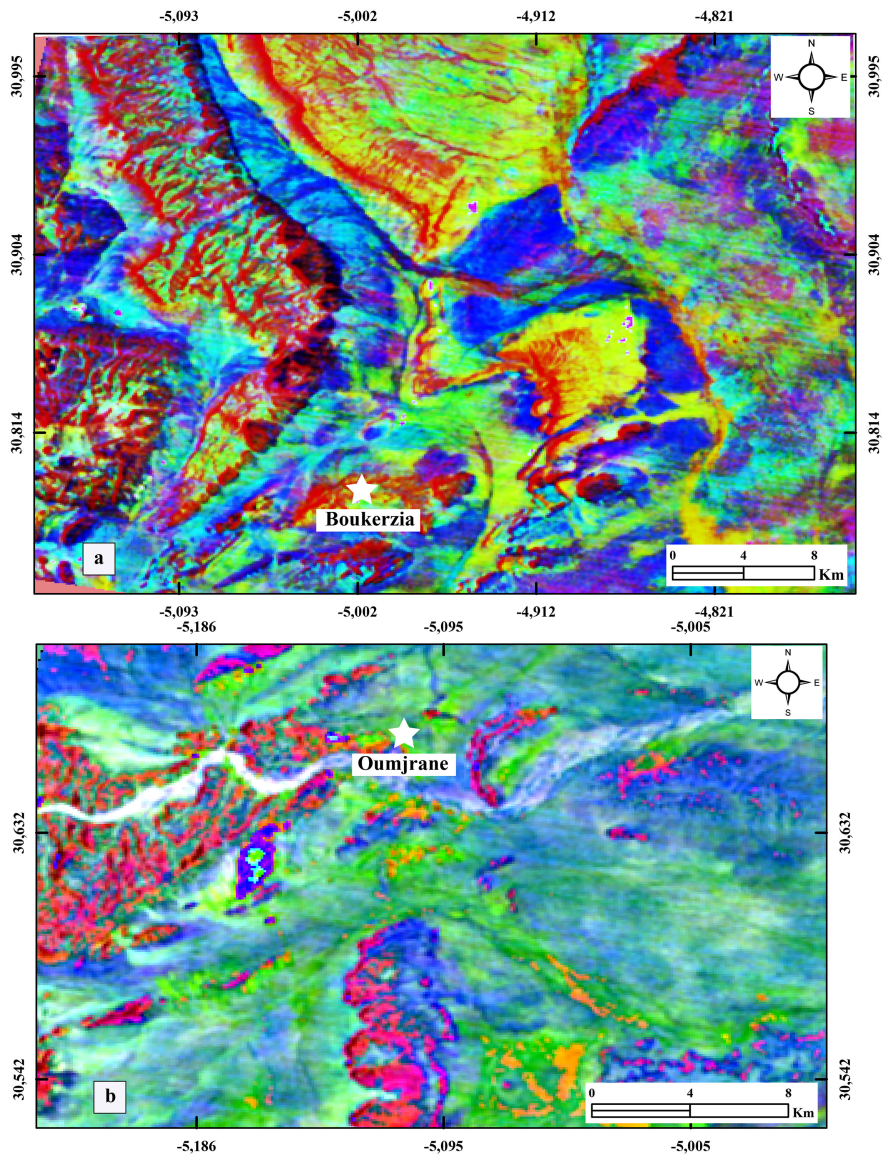

Figure 4. RGB component from ASTER image processing: (a) RGB (PC5, PC4 and PC3) Boukerzia zone; (b) RGB (PC6, PC4 and PC1) Bounhas zone.

two absorption phases (low reflectance) belongs to the 0.4 to 0.9 µm spectral region [17]. The results obtained from band ratios combination (b5/b3 + b1/b2) are very effective in detecting areas of a high concentration of iron oxide and hydroxide minerals. They are marked by a red color in the map of iron oxide and hydroxide zones, whose spatial distribution is illustrated in **Figure 5(a)**. The analysis of the spectral response resulting from this processing shows that these zones present a significant reflectance in the intervals of 0.5 to 0.8 um, 1.0 to 1.3 um and 1.4 to 1.5 um. Moreover, the pixels that are rich in ferric iron (Fe^{3+}) show significant absorption of 0.6 to 0.63 um and 1.5 um spectral region **Figure 5(a2)**. The characteristics of the spectral reflectance of these pixels in comparison with the spectral library of iron oxides and hydroxides coincide with the alteration minerals, such as jarosite, limonite and hematite **Figure 5(a1)**. These minerals are very abundant in the study area, whose origin is linked to the alteration of the primary ore like the pyrite. The details of the spectral characteristics of each of these minerals are presented as follows:

- **Limonite:** it is formed by a superficial alteration of several iron minerals especially (siderite, magnetite and pyrite) in association with clays. The limonite is known by its brown or yellowish color. It represents the main component ore of gossan, whose spectral characteristics are more common to goethite (Figure 5(b)), and it is characterized by a particular absorption in the VNIR region due to electronic transitions of ferric iron, indicated by a very important absorption peak in the electromagnetic spectrum of 0.63 um with two intervals of significant reflectance from 0.45 to 0.5 um and another about 1.25 to 1.3 um region (Figure 5(c)).

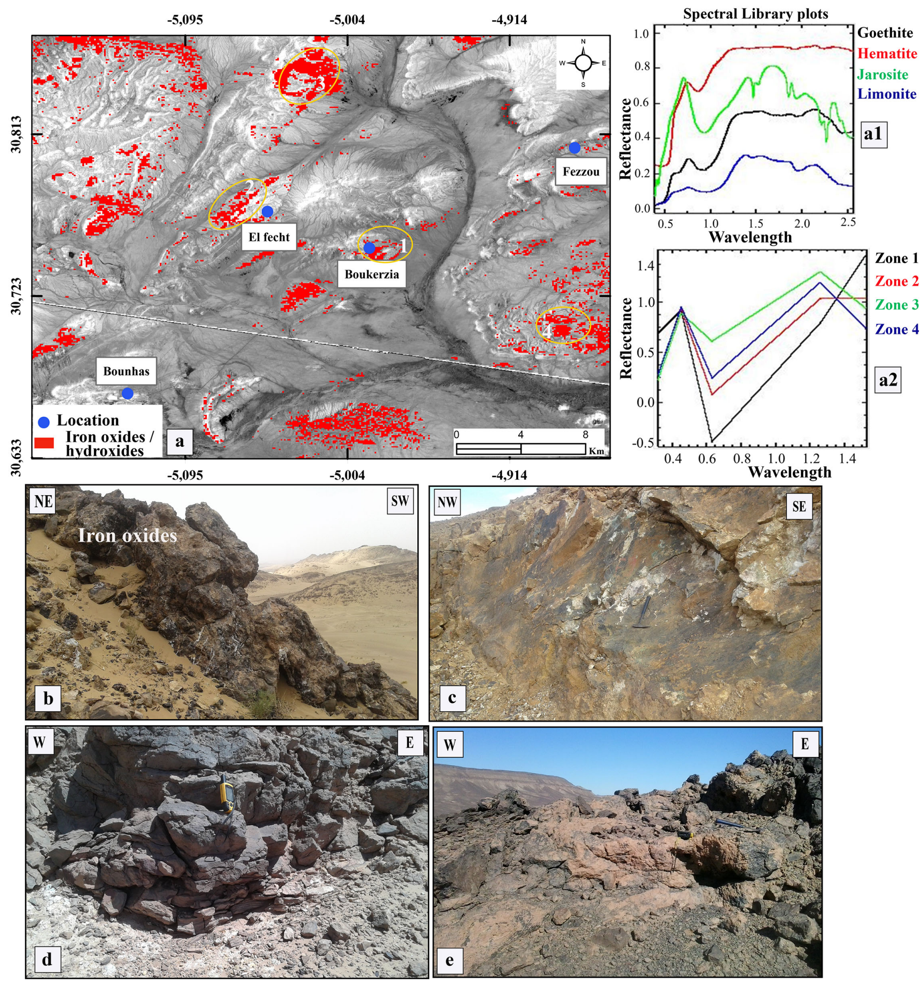

Figure 5. Surfaces of iron oxide minerals detected during the processing of the ASTER image covering the Oumjrane-Boukerzia region: (a) superimposition of the surfaces detected with PC8; (a1) USGS spectral libraries of iron oxide and hydroxide minerals; (a2) spectral signatures of a few pixels belongs to areas rich in iron oxides and hydroxides; (b) photo taken in the Boukerzia area (zone 1); (b1) hematite-rich gossan; (c) photo taken from the El fecht fault (zone 2); (c1) limonite-rich gossan; (d), (e) second Bani sandstone (zone 3 and zone 4); (d1), (e1) sandstone rich in iron oxide (Jarosite).

- **Jarosite:** It is a hydrous iron mineral, present in acid environments rich in sulfates formed by the oxidation of sulfides in particular pyrite (FeS_2). It has the spectral characteristics of absorption in the wavelength recorded in the VNIR, SWIR spectral region (0.62 um and 1.5 um). This mineral displays a remarkable reflectance in the 0.5 to 0.55 um and 1.25 to 1.3 um regions, sometimes diagnostic vibrational absorptions in the SWIR. In the study area, the Jarosite is generally concentrated in the sandstone surfaces, and frequently in the wall rock zones of the mineralized veins (**Figure 5(a)**).
- **Hematite:** corresponds to the main iron oxide minerals in the study area. Tne hematite appeared mainly with an ocher color to rust. It is marked by a remarkable reflectance in band 4 (1.65 um) and a low reflectance in band 2 (0.62 um) (**Figure 5(c)**).

The data obtained from ASTER image processing and the analysis of the samples taken directly from the field during the fieldwork verification of the results, make it possible to deduce that these iron oxides and hydroxides minerals are outcropped in the form of gossan, their origin is mainly linked to the alterations of the primary minerals represented by pyrite and magnetite. In addition, the gossan outcrops generally follow the directions of the mineralized veins (Cu, Pb and Ba), exposed at the Oumjrane-Boukerzia mining region (**Figure 5(a)**). In addition, some pixels are manifested in the form of surfaces, especially in the northwestern part of the study area, these surfaces are occupied by geological formations belonging to the Upper Ordovician sedimentary pile (sandstone of second Bani) (**Figure 5(d)**). These lithological units are designated as the main host of the mineralization (Cu, Pb, Ba) of Oumjrane-Boukerzia, whose occurrence is characterized by very high concentrations of ferric iron, which allows them to be distinguished as pixels rich in iron oxide minerals (**Figure 5(e)**).

5.2. Quartz Index (QI)

The quartz index (IQ) is widely used in geological mapping and the investigation of mineral resources by satellite images, specifically the ASTER imagery. This index has been implemented by the spectral bands of ASTER TIR, because the rock formations rich in quartz elements present a very important absorption of SiO_2 in the TIR domain [18] [19]. This index is defined by the following formula:

$$\text{Quartz Index (QI)} = (b11 * b11)/(b10 * b12)$$

(b10: band 10; b11: band 11; b12: band 12)

The results obtained in this report are more effective in identifying formations rich in SiO_2 (**Figure 6(a)**). They are marked by two reflectance peaks in the wavelength of the order of 9.25 µm, 10.7 µm, with a selective absorption in the 8.6 µm, which corresponds to the band 11 (**Figure 6(a1)**). Indeed, these quartz-rich zones are generally located along of the mineralized faults (Cu, Pb and Ba), especially in the north of Jbel Boukerzia and the eastern part of Fezzou (zone 1). Moreover, the geological formations rich in quartz (quartzitic sandstone) are manifested by a set of pixels, presented in the form of surfaces, especially in the northwestern zone (zone 2) and the southwestern part (zone 3), these zones are well illustrated in **Figure 6(a2)**. After verification throughout several fieldwork missions, it is worth noted that these clear zones correspond to the formations of quartzite sandstones of the second Bani (Upper Ordovician) that are rich in quartz (**Figure 6(c)**, **Figure 6(e)**). as well as the sedimentary formations which contain a large quantity of the SiO_2 elements due to the presence of late quartz (white quartz), these elements have the same spectral characteristics of primary quartz, generally associated with mineralized structures in the area. It is considered to be the most important indicator in the process of hydrothermal mineralization (Cu, Pb, Ba) currently exploited in the Oumjrane-Boukerzia area (**Figure 6(b)**, **Figure 6(d)**).

5.3. Index of Carbonate Minerals

In order to identify carbonate surfaces we have used b7/b5 + b8/b4 band ratios combination. The obtained results show that the carbonated zones occupy a large surface in the north-eastern part of the study region (zone 2), and small surfaces

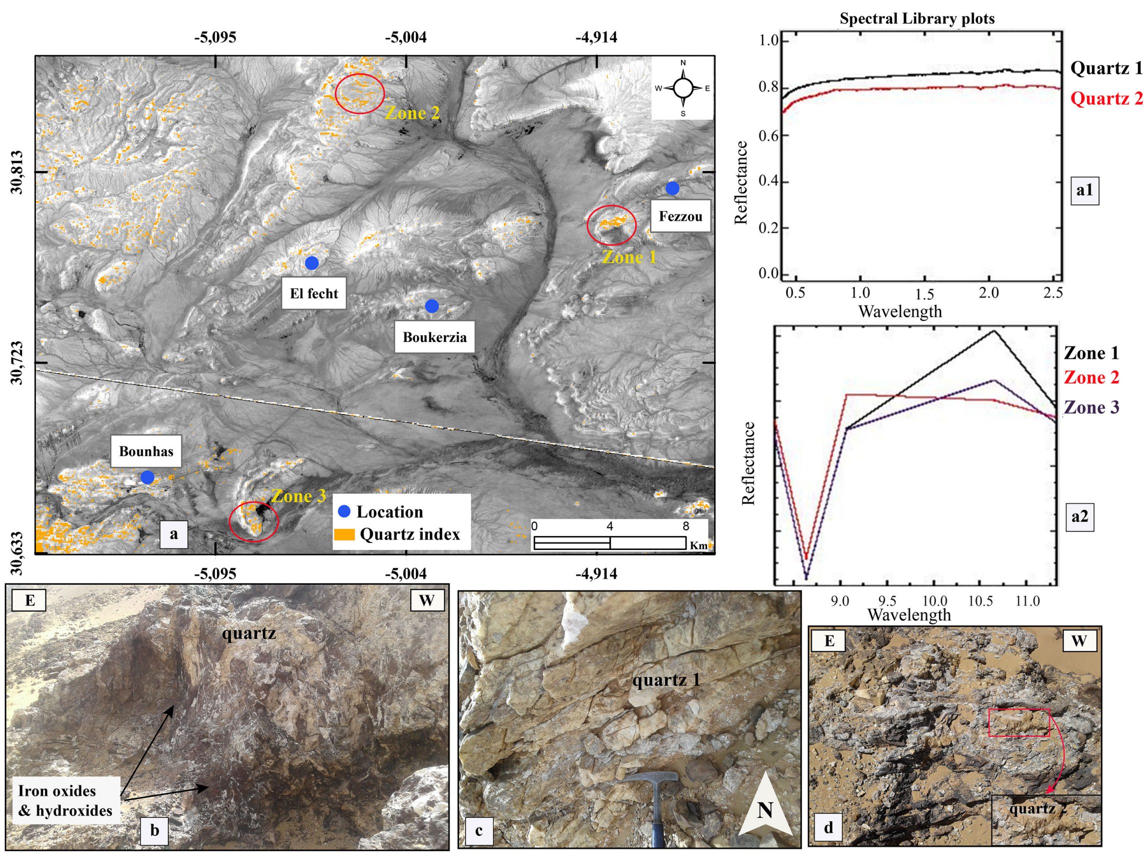

Figure 6. The quartz index (a) superimposition of the quartz index calculated with PC8 of the ASTER image; (a1) quartz spectral signature from the USGS library; (a2) spectral angle mapper (SAM) extracted in SiO2-rich pixels; (b), (d) quartz vein, North-East of Jbel Boukerzia; (b1) quartz elements constitute the northeast vein of Boukerzia; (c) quartz vein, southeast of Jbel Bounhas; (c1) sample rich in quartz elements and iron oxide; (e) quartzite sandstones of the second Upper Ordovician Bani; (e1) sample rich in white quartz.

are manifested in the southern part of Jbel Bounhas (zone 3) and at the east of Jbel rich Merzoug (zone 1) (**Figure 7(a)**). The extraction of the spectral signature in the different pixels which reflect the indices of carbonate minerals in these zones, has based on the fact that the carbonate is characterized by two absorption intervals in the SWIR domain, one in the wavelength from 2.25 to 2.30 µm (band 7) and the other about 2.31 to 2.35 µm (band 8) (**Figure 7(a2)**). The comparison between the absorption characteristics of the identified pixels with the spectral responses recorded in the USGS (United States Geological Survey) spectral library, makes it possible to distinguish between the main minerals constituting the carbonate formations such as dolomite ($MgCa(CO_3)_3$), with significant absorption in the 2.25 µm wavelength, calcite ($CaCO_3$) about 2.33 µm, this absorption is due to the presence of high concentrations of CO_3 (**Figure 7(a1)**).

On the basis of geological map of Todgha-Maider, covering the study area with field data as a validation process tool for these results, allow us to deduce that the set of associated pixels in the northeastern part of the area correspond to the spectra of dolomite, very abundant in Devonian limestone formations (**Figures 7(b)-(d)**). On the other hand, the spectrum of calcite is very developed in the south-western part, this zone was marked by the presence of quaternary formations due to alluvial deposits (**Figure 7(e)**).

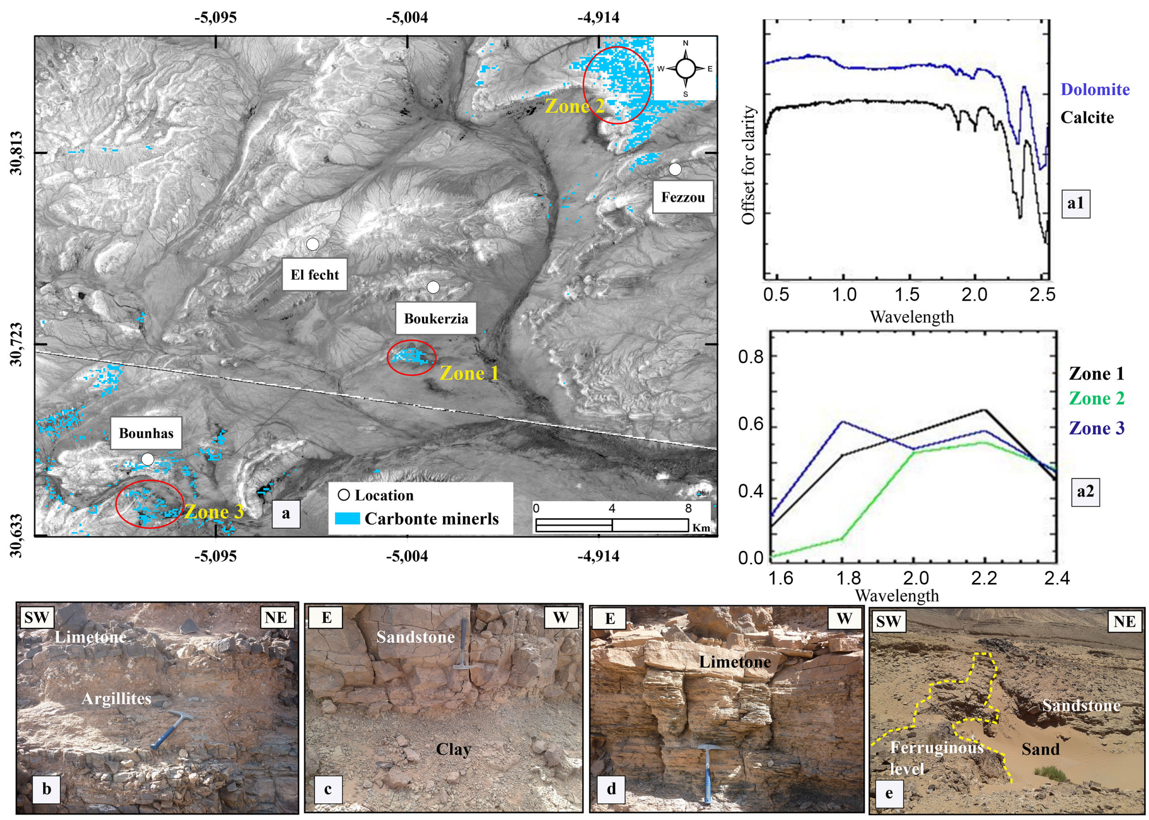

Figure 7. Carbonate mineral index: (a) carbonate minerals identified from the ASTER image; (a1) USGS spectral library of dolomite and calcite; (a2) spectral pixel signature of carbonate minerals; (b) the lower Devonian dolomites, east of Rich Merzoug; (c), (d) Middle Devonian limestones; (c1) traces of fossils; (e) limestone formations, south of Jbel Bounhas

5.4. Clay Mineral Index

The clay minerals depict significant spectral response in the SWIR domain [20] [21] [22]. Indeed, the display of spectra from the USGS (United States Geological Survey) library (**Figure 8(a1)**) that corresponds to the clay minerals, allowed us to choose the band ratios combinations that can be useful to identify these minerals, such as (B4 + B6/B7)/(B8 + B9/B5). The obtained results are very effective in identifying the intervals of the spectral signatures corresponding to the pixels of the clay minerals illustrated in the resulting image, which are marked by the green color (**Figure 8(a)**). The extraction of the spectral signatures of different identified pixels (**Figure 8(a2)**), in comparison with pre-existing data (reports, geological map, etc.), allowed us to deduce the nature of the clay minerals abundant in the area. These results show that the spectral characteristics of the majority of the resulting new pixels coincide with the spectral responses of the following minerals:

- **Chlorite:** It is marked by a high reflectance in the bands 5 and 8, while it has a low reflectance in band 9, recorded in zone 1, **Figure 8(a2)**. The high values of this index appeared in the pixels in green color, all of these pixels represent the formations associated with an enrichment of micas such as muscovite and biotite, which are particularly abundant in greenish shales (ktaoua shales of Upper Ordovician age). Their occurrences are illustrated in **Figure 8(b)**.

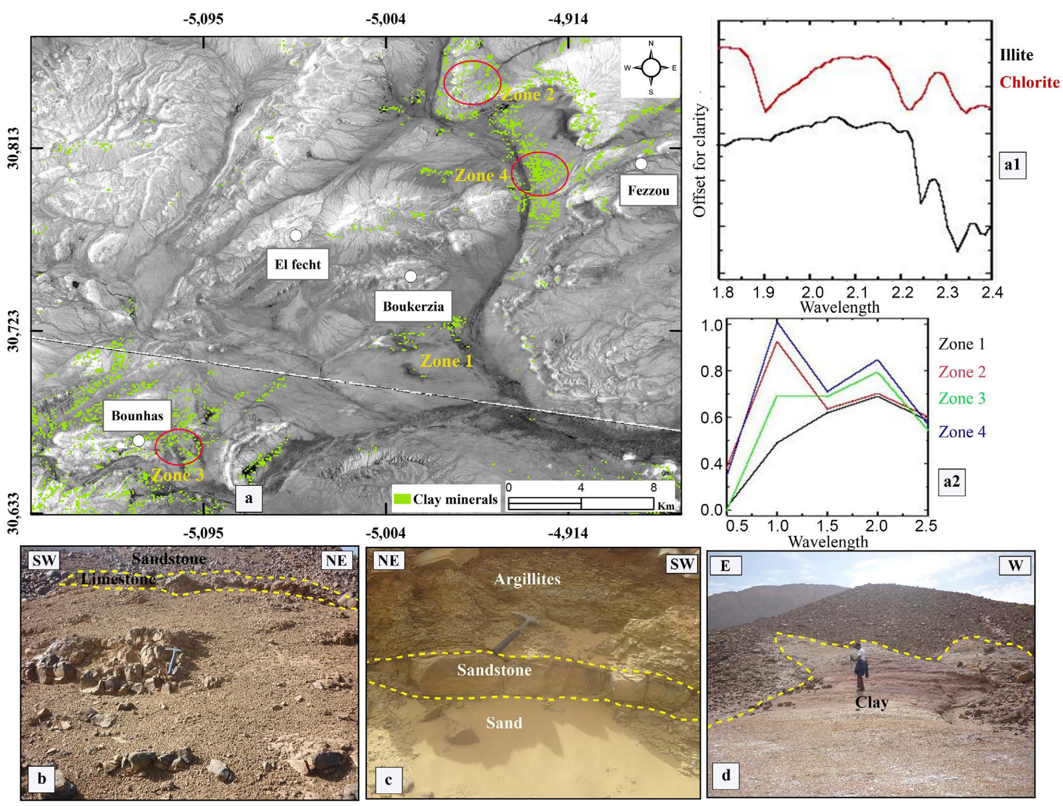

Figure 8. The index of clay minerals: (a) surfaces identified from the ratios of the spectral bands of the ASTER images; (a1) spectral profile of clay minerals; (a2) spectral signatures extracted in the pixels correspond to clay minerals; (b) the clay minerals within the eastern zone of the Rich Merzoug; (c) clay minerals at the northeast part of Boukerzia zone; (d) Middle Devonian clays.

- **Illite, Kaolinite:** they are very common minerals in sediments, soils and clayey sedimentary rocks and sometimes in some low-grade metamorphic rocks, whose spectral features appeared in the SWIR region. They are marked by a high reflectance in bands 5 and 8 with two absorption intervals recorded in bands 4 and 9 (zone 2, 3 and 4) (Figure 8(c), Figure 8(d)). These four bands have been used in the band ratio processing as the input data for the purpose of distinguishing these minerals from others that do not correspond to clay minerals.

The results were verified in the field, after the selection of the coordinates (X, Y) of different resulting pixels from ASTER data processing. The data are taken from the field show that the identified surfaces are mainly occupied by clay formations. These two clays mineral zone is illustrated by the Figure 8.

6. Discussion

This study shows that remote sensing data and the fieldwork investigations are powerful tools and suitable in identifying the hydrothermal alteration zones.

The combination between the results of the indices of the minerals calculated in a single image, makes it possible to identify the spatial distribution of hydrothermal alteration mineral zones. This resulting map can be used as an important reference for mining exploration in the Oumjrane-Boukerzia region. Indeed, several types of minerals have been detected during the reports of the spectral bands applied to the ASTER image, these resulting surfaces were superimposed with the main faults, affected the study area, whose distribution was presented in Figure 9. Analyzing the map of Figure 9, we notice the main alterations mineral zones are occurred and mostly coincide to the mapped faults and fractures. The results of the band ratios used in these types of processing allowed us to distinguish between four families of minerals abundant in the study area, distributed as follows:

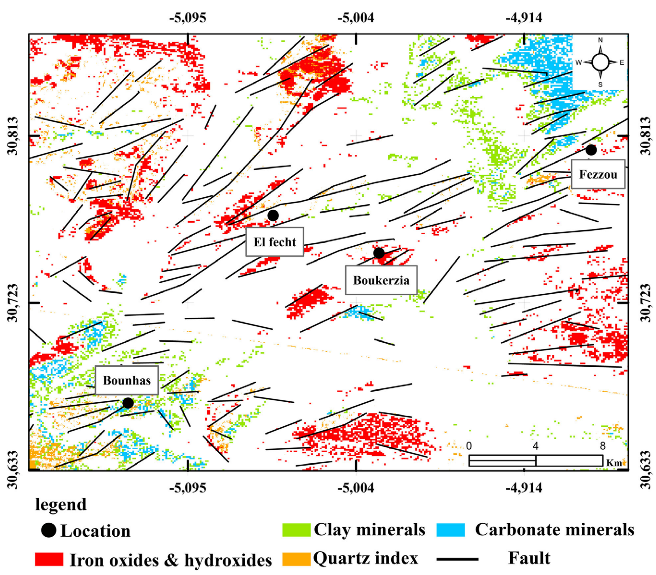

Figure 9. Map of hydrothermal alterations obtained from the spectral band ratios applied to the ASTER images

- **Iron oxide/hydroxide minerals:** they are marked by red pixels that occupy large areas. In some places, these areas correspond the many ferruginous surfaces and level interbedded in the first Bani and second Bani sedimentary formations. These formations are characterized by very high concentrations of iron minerals, which explains the appearance of these pixels in the form of small areas, especially the northwestern area of the study area. In general, these iron oxides and hydroxides zones are aligned with the directions of the faults and mineralized veins.
- **Carbonate minerals rich in CO3:** they are illustrated by the open blue color, these minerals are concentrated in the northeastern part and the south-western part of the study area, of which the exposure of the formations of Devonian carbonates is very dominant.
- **The quartz index:** the quartz mineral zones, are manifested in the south-western zone, especially the south of Jbel Bounhas. They are less outcropped in the north-western part of the study area. The pixels that are correspond to quartz minerals zones are marked in yellow color.
- **Clay minerals**: the surfaces correspond to these minerals have been identified in the north-eastern and south-western part of the study region. These areas are mainly occupied by quaternary formations which are dominated by clays. Their occurrences appear in green color

As the region is characterized by several mineral zones, mainly in a form of veins [5], the use of remote sensing for delineating altered mineral zones has become important and valuable for mineral exploration [22]. This study shows that a significant coincidence of mapped lineaments on the identified zones of hydrothermally altered minerals. It is worth noting that, after several fieldwork missions, the iron oxides and hydroxides are closely related the mineral veins in the region, except in some tiny ferruginous levels that are interbedded in the Ordovician sedimentary series. The fact that the iron oxides and hydroxides are ultimately related the minerals veins is suggested in several districts along the Tafilalet and Maider Paleozoic basins at the extreme eastern part of the Anti-Atlas belt [11] [12].

7. Conclusion

Through the present paper, we have set up a methodology for geological mapping based on multi-source remote sensing data, especially ASTER data. In this case we used satellite image processing techniques, mainly the method of band ratios, principal component analysis and colored composition. The obtained results in these treatments have succeeded in identifying the areas that have undergone strong hydrothermal alterations in the Oumjrane-Bouerzia area. The analysis of the spectral response of the resulting pixels in the band ratio technique, allowed us to deduce the nature of the dominant alteration minerals in the area, in particular iron oxides and hydroxides, which are mostly coincided with the main fault zones of the study area. The spectral signatures of clay minerals, such as kaolinite, illite and chlorite, are recorded mainly in the SWIR domain, these carried out band ratios, have allowed us to identify the carbonate minerals including calcite, dolomite, especially in the SWIR bands. ASTER thermal data can be used to map the quartz minerals occurrences. Consequently, the comparison of the obtained results from the processing of satellite data with pre-existing data (report, geological map, etc.), geological fieldwork, laboratory studies, have made it possible to determine and delimit the areas of alterations potentially favorable to mineral exploration, especially the remote and inaccessible zones.

Acknowledgements

The authors would like to thank of the scientific research teams "Applied Geology, Environmental Geomatics" and "Applied Geodynamics and Remote Sensing in Natural Resources" from the Department of Geology at Hassan II University of Casablanca, Morocco, for supporting this work. We would like also to thank also all members of the Oumjrane Mining Company's geological department, as well as AKKA Gold Mining, MANAGEM GROUP, for their efficient guidance and assistance throughout our internship. The authors are very grateful to the reviewers of Journal and the Technical Editors for their great efforts and valuable comments.

Conflicts of Interest

The authors declare no conflicts of interest regarding the publication of this paper.

References

[1] Deroin, J.-P. (2019) An Overview on 40 Years of Remote Sensing Geology Based on Arab Examples. In: Bendaoud, A., Hamimi, Z., Hamoudi, M., Djemai, S. and Zoheir, B., Eds., *The Geology of the Arab World—An Overview*, Springer Geology. Springer International Publishing, Cham, 427-453. https://doi.org/10.1007/978-3-319-96794-3_12

[2] Ouhoussa, L., Ghafiri, A., Benaissi, L., Es-Sabbar, B. and Si Mhamdi, H. (2022) Lithostructural Mapping Using Landsat OLI images and Field Investigations in the Oumjrane-Boukerzia Mining District, Eastern Anti-Atlas, Morocco. *Iraqi Geological Journal*, **55**, 14-33. https://doi.org/10.46717/igj.55.2C.2ms-2022-08-15

[3] Gasmi, A., Gomez, C. and Zouari, H. (2016) PCA and SVM as Geo-Computational Methods for Geological Mapping in the Southern of Tunisia, Using ASTER Remote Sensing Data Set. *Arabian Journal of Geosciences*, **9**, Article No. 753. https://doi.org/10.1007/s12517-016-2791-1

[4] El Ghrabawy, O., Soliman, N. and Tarshan, A. (2019) Remote Sensing Signature Analysis of ASTER Imagery for Geological Mapping of Gasus Area, Central Eastern Desert, Egypt. *Arabian Journal of Geosciences*, **12**, Article No. 408. https://doi.org/10.1007/s12517-019-4531-9

[5] Boissavy, C. (1979) Etude Structurale et Métallogénique des filons cuprifères du Maider Occidental (Anti-Atlas Marocain). Paris, 219.

[6] Destombes, J. (2006) Carte géologique au 1/200 000 de l'Anti-Atlas marocain, paléozoïque infér, cambrien moyen supér, ordovicien-Base silurien Somm. Général Sur

Mém. Explic. Cartes Géologiques Au 1, 000

[7] Destombes, J. (1962) Stratigraphie et paléogéographie de l'Ordovicien de l'Anti Atlas Maroc un essai de synthèse. *Bulletin de la Société Géologique de France*, **7**, 453-460. https://doi.org/10.2113/gssgfbull.S7-IV.3.453

[8] Du Dresnay, R., Hindermeyer, J., Emberger, A., Caia, J., Destombes, J. and Hollard, H. (1988) Carte Géologique du Maroc au 1: 200 000. Feuille Todgha—M'aider, and Notice explicative. Notes et Mémoires du Service Géologique du Maroc, 243, & 243 bis.

[9] Baidder, L. (2007) Structuration de la bordure septentrionale du Craton Ouest Africain du Cambrien à l'actuel: Cas de l'Anti-Atlas oriental du Maroc. Université Hassan II, Casablanca, 209 p.

[10] Kharis, A. (2015) Etude géologique, gîtologique et métallogénique des minéralisations cuprifères du district minier d'Oumjrane (Anti-Atlas oriental, Maroc). Université Moulay Ismail, Meknès, 311 p.

[11] Es-Sabbar, B., Essalhi, M., Essalhi, A. and Mhamdi, H.S. (2020) Lithological and Structural Lineament Mapping from Landsat 8 OLI Images in Ras Kammouna Arid Area (Eastern Anti-Atlas, Morocco). *Economic and Environmental Geology*, **53**, 425-440.

[12] Ait Daoud, M. (2021) La minéralisation filonienne à Pb, Zn, Cu et barytine de l'anticlinal de Tadaout-Tizi n'Rsas (Anti-Atlas oriental, Maroc): Evolution géodynamique et contribution métallogénique. Université Moulay-Ismaïl, Meknès, 242 p.

[13] Robert-Charrue, C. (2006) Géologie structurale de l'Anti-Atlas oriental, Maroc. Université de Neuchâtel, Neuchâtel, 224 p.

[14] Burkhard, M., Caritg, S. and Helg, U. (2006) Tectonics of the Anti-Atlas of Morocco. *Comptes Rendus Geoscience*, *338*, 11-24. https://doi.org/10.1016/j.crte.2005.11.012

[15] Baidder, L., Raddi, Y., Tahiri, M. and Michard, A. (2008) Devonian Extension of the Pan-African Crust North of the West African Craton, and Its Bearing on the Variscan Foreland Deformation: Evidence from Eastern Anti-Atlas (Morocco). *Geological Society*, *London*, *Special Publications*, **297**, 453-465. https://doi.org/10.1144/SP297.21

[16] El Janati, M. (2019) Application of Remotely Sensed ASTER Data in Detecting Alteration Hosting Cu, Ag and Au Bearing Mineralized Zones in Taghdout Area, Central Anti-Atlas of Morocco. *Journal of African Earth Sciences*, **151**, 95-106. https://doi.org/10.1016/j.jafrearsci.2018.12.002

[17] Hung, L.Q., Batelaan, O. and De Smedt, F. (2005) Lineament Extraction and Analysis, Comparison of LANDSAT ETM and ASTER Imagery. Case Study: Suoimuoi Tropical Karst Catchment, Vietnam. In: Ehlers, M. and Michel, U., Eds., Proceedings *Remote Sensing for Environmental Monitoring*, *GIS Applications*, *and Geology V*, Vol. 5983, International Society for Optics and Photonics (SPIE), Bellingham. https://doi.org/10.1117/12.627699

[18] Pour, A.B., Hashim, M. and van Genderen, J. (2013) Detection of Hydrothermal Alteration Zones in a Tropical Region Using Satellite Remote Sensing Data: Bau Goldfield, Sarawak, Malaysia. *Ore Geology Reviews*, **54**, 181-196. https://doi.org/10.1016/j.oregeorev.2013.03.010

[19] Safari, M., Maghsoudi, A. and Pour, A.B. (2018) Application of Landsat-8 and ASTER Satellite Remote Sensing Data for Porphyry Copper Exploration: A Case Study from Shahr-e-Babak, Kerman, South of Iran. *Geocarto International*, **33**, 1186-1201. https://doi.org/10.1080/10106049.2017.1334834

[20] Eldosouky, A.M., Abdelkareem, M. and Elkhateeb, S.O. (2017) Integration of Remote Sensing and Aeromagnetic Data for Mapping Structural Features and Hydrothermal Alteration Zones in Wadi Allaqi Area, South Eastern Desert of Egypt. *Journal of African Earth Sciences*, **130**, 28-37. https://doi.org/10.1016/j.jafrearsci.2017.03.006

[21] Mars, J.C. and Rowan, L.C. (2006) Regional Mapping of Phyllic- and Argillic-Altered Rocks in the Zagros Magmatic arc, Iran, Using Advanced Spaceborne Thermal Emission and Reflection Radiometer (ASTER) Data and Logical Operator Algorithms. *Geosphere*, **2**, 161-186. https://doi.org/10.1130/GES00044.1

[22] Amer, R., Kusky, T and Ghulam, A. (2010) Lithological Mapping in the Central Eastern Desert of Egypt Using ASTER Data. *Journal of African Earth Sciences*, **56**, 75-82. https://doi.org/10.1016/j.jafrearsci.2009.06.004